Supplementary Materials for "Feasibility of Deep Learning in Shear Wave Splitting analysis: Synthetic-Data Training and Waveform Deconvolution"

Megha Chakraborty [1, 2], **Georg Rümpker** * [1,2], **Wei Li**[1], **Johannes Faber**[1, 3], **Frederik Link** [4], **Nishtha Srivastava** [1,2]

[1]Frankfurt Institute for Advanced Studies, 60438 Frankfurt, Germany, [2]Institute of Geosciences, Goethe University Frankfurt, 60438 Frankfurt, Germany, [3]Institute for Theoretical Physics, Goethe University Frankfurt, 60438 Frankfurt, Germany, [4]The Department of Earth & Planetary Sciences, Yale University, New Haven CT 06511, United States

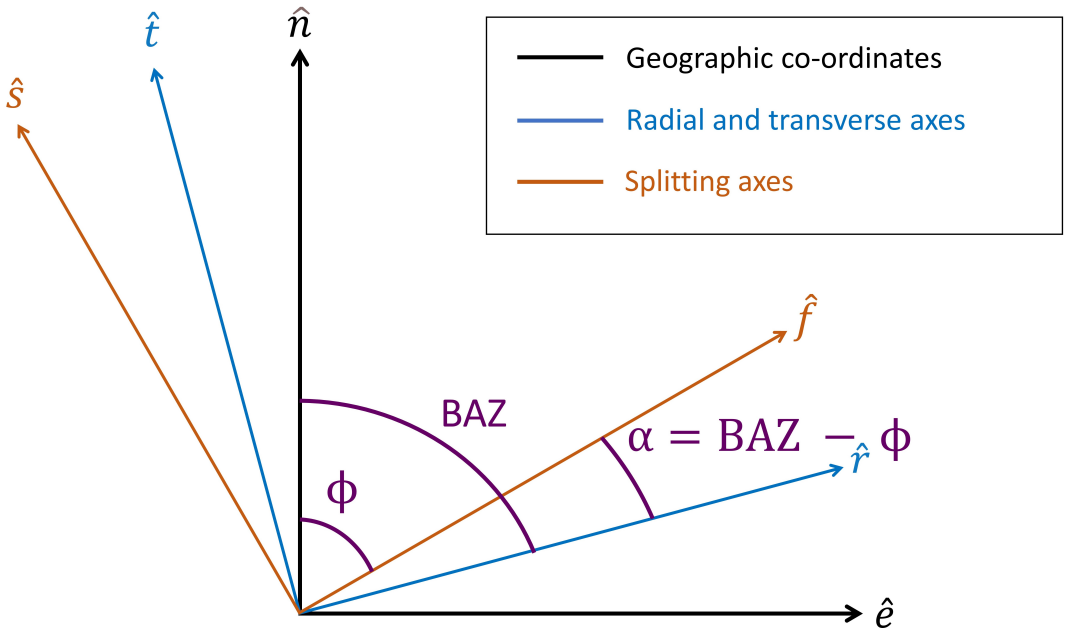

Figure S1 Co-ordinate system used for the derivation of equations 1-5.

*Corresponding author: rumpker@geophysik.uni-frankfurt.de

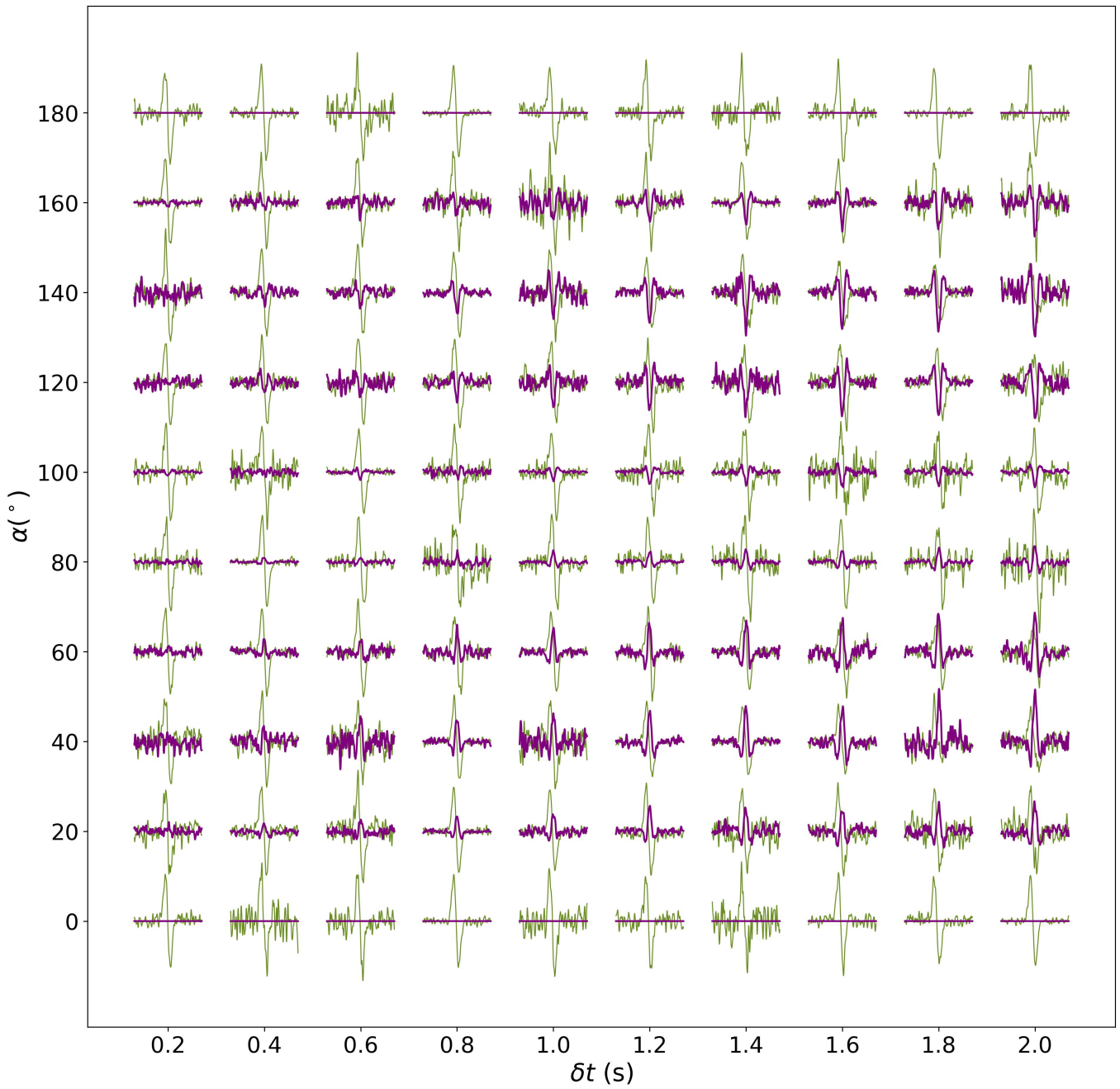

Figure S2 Examples of synthetic data contaminated with random noise for different α and δt pairs. The olive line represents the radial component while the purple line represents the transverse component. The noise is added independently to the fast and slow components and the noise level is chosen from a random normal distribution with mean 30% and standard deviation 10%.

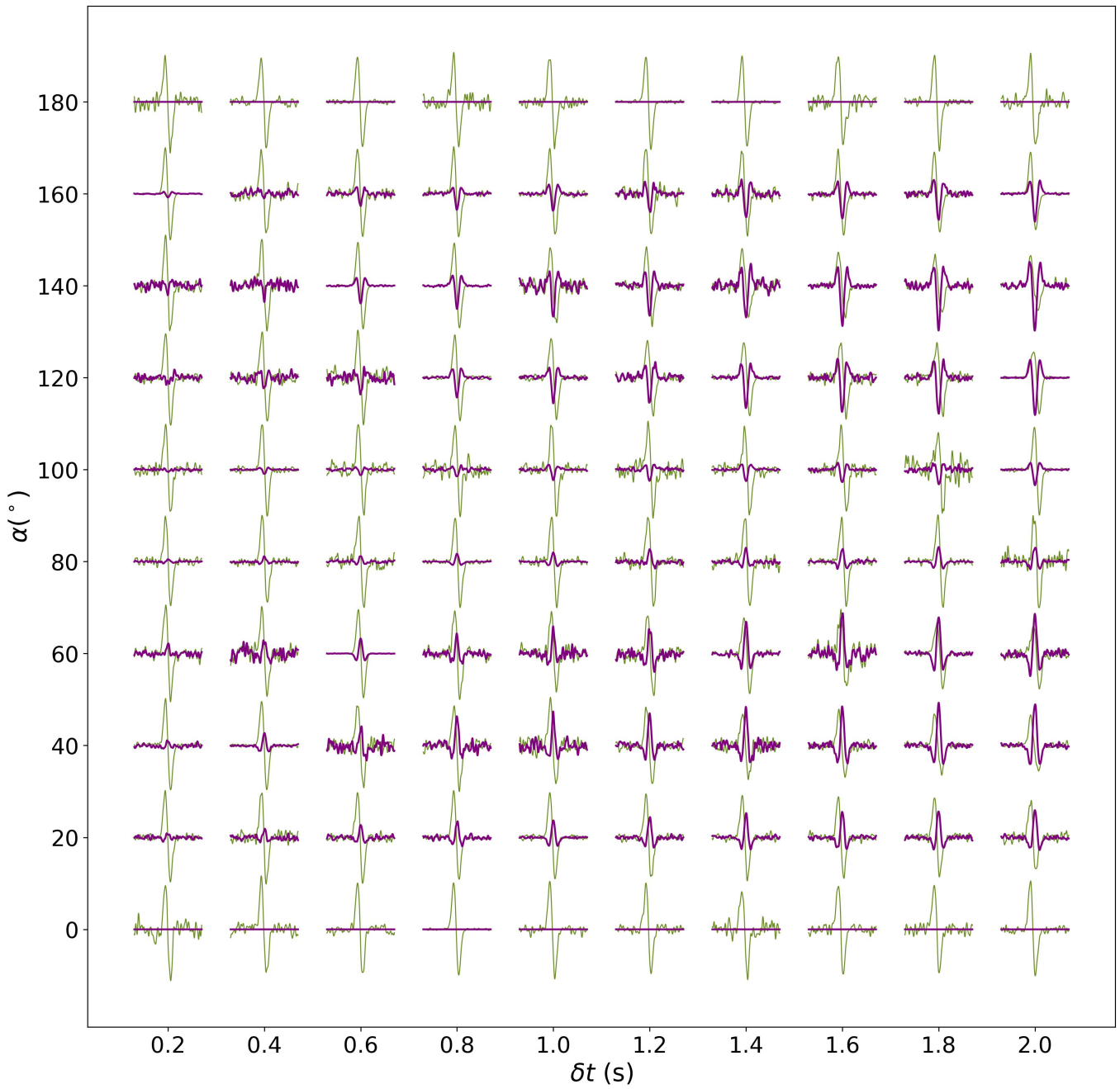

Figure S3 Examples of synthetic data contaminated with gaussian noise for different α and δt pairs. The olive line represents the radial component while the purple line represents the transverse component. The noise is added independently to the fast and slow components and the noise level is chosen from a random normal distribution with mean 30% and standard deviation 10%.

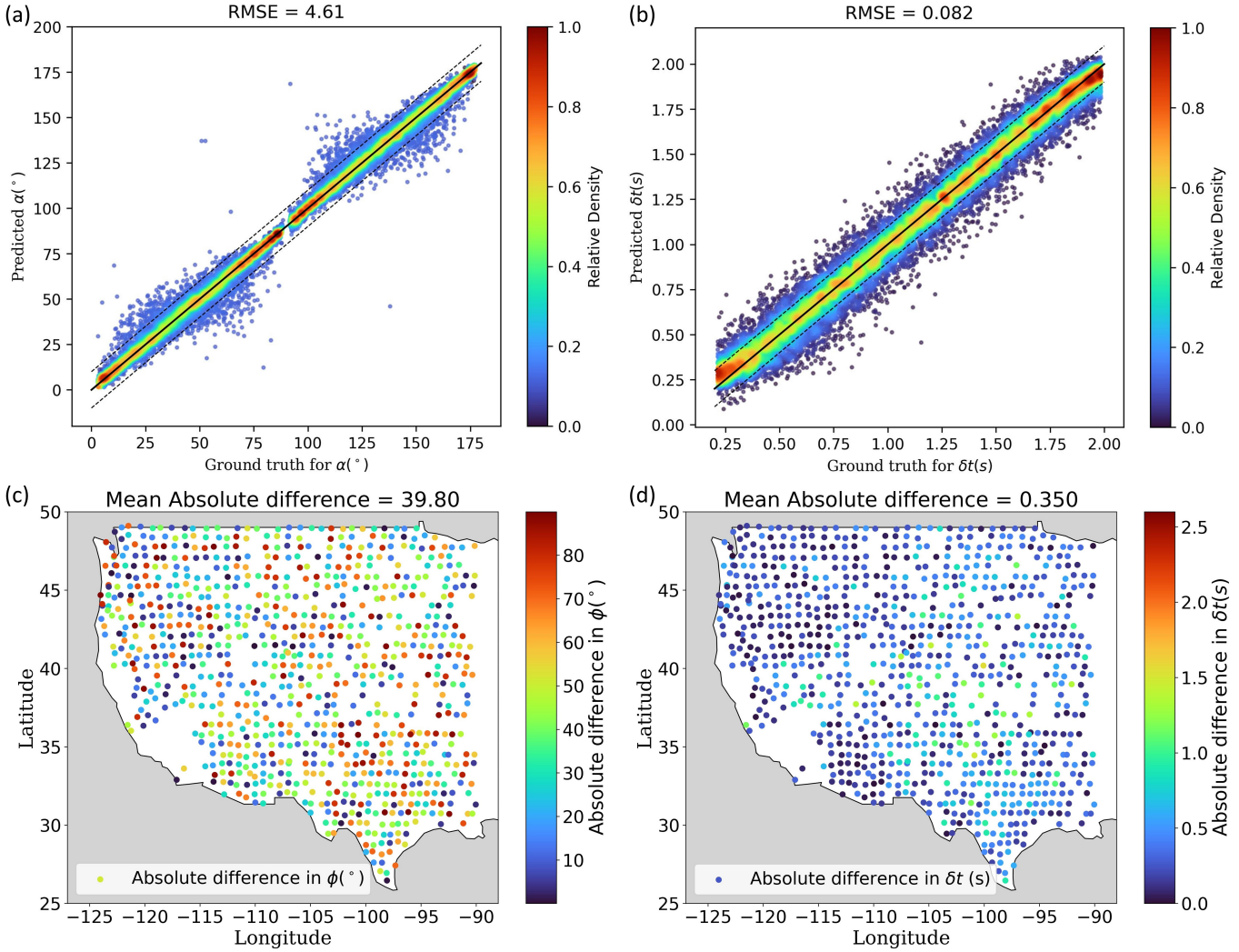

Figure S4 The relation between ground truth and predictions for (a) α and (b) δt when model trained on synthetic training data contaminated with gaussian noise is tested on synthetic test data contaminated by gaussian noise; comparison between station-wise averages of (c) α and (d) δt calculated using the deep learning model and those given by Liu et al. (2014)

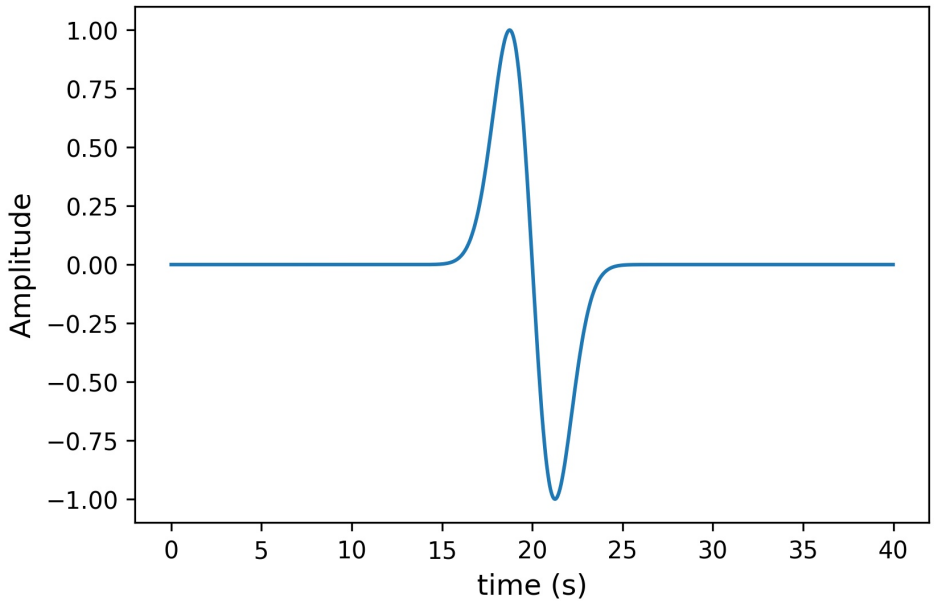

Figure S5 The normalized derivative of an exponential function.

The following equations are used to define the function given in Figure S5:

$$T_{eff} = 0.1 \times 2\pi T \tag{S1}$$

$$wave_{norm} = \frac{4}{T_{eff}\sqrt{e}} \tag{S2}$$

$$wave = -\frac{16}{T_{eff}^2} \times \frac{(t-t0)e^{-\frac{8}{T_{eff}^2}(t-t0)^2)}}{wave_{norm}} \tag{S3}$$

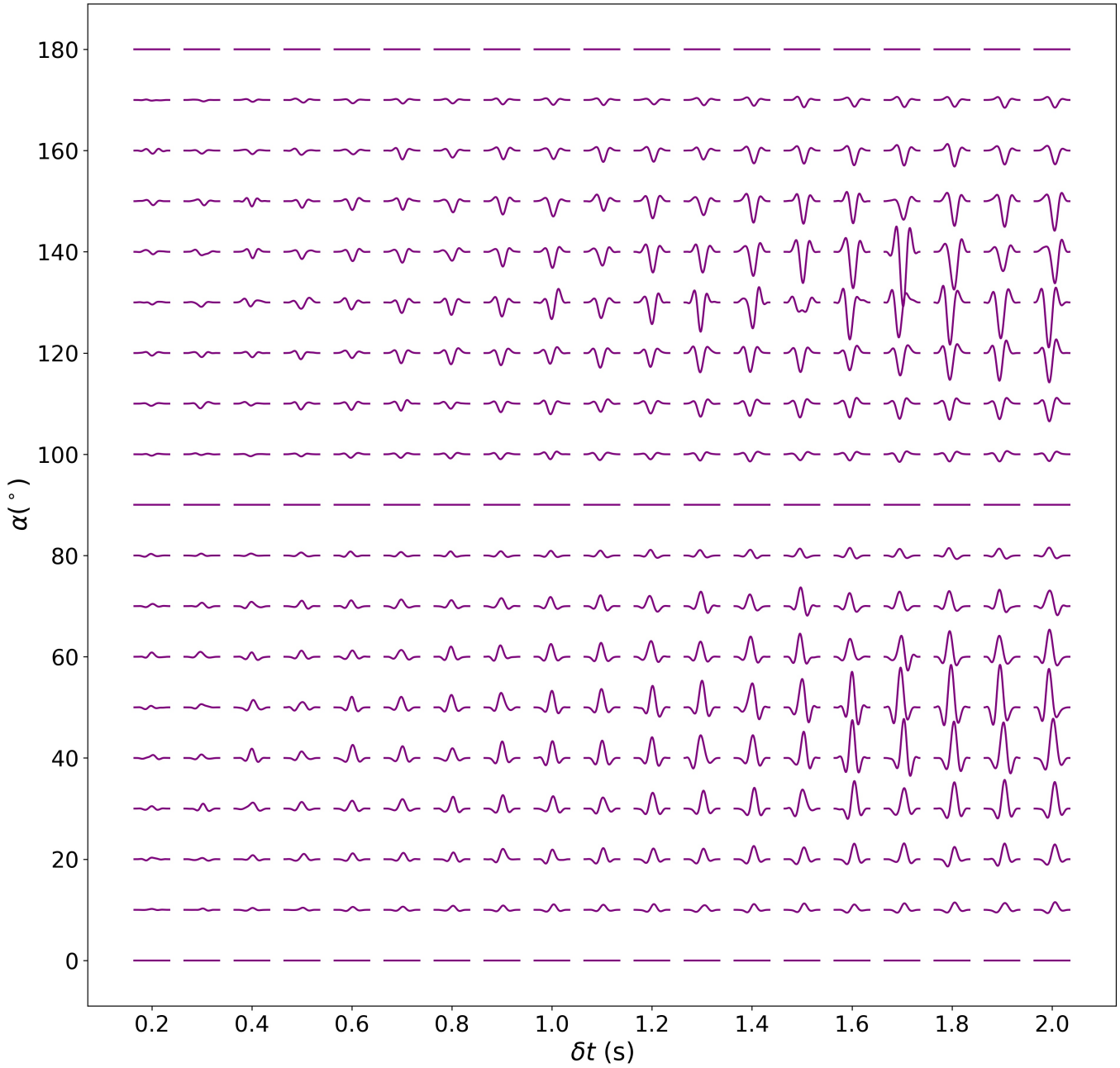

Figure S6 Pre-processed transverse components for different combinations of α and δt

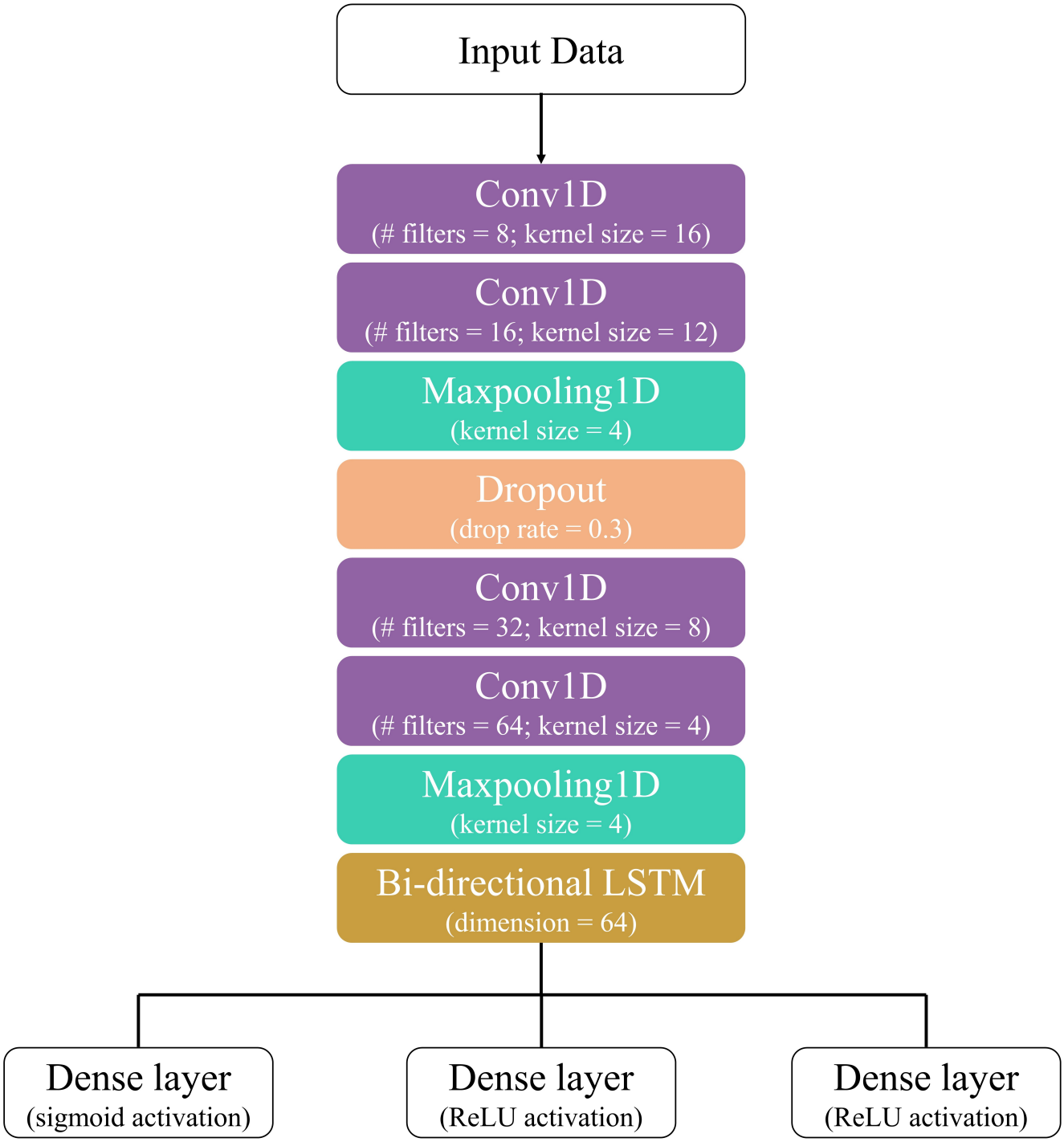

Figure S7 A detailed overview of the SWSNet architecture.

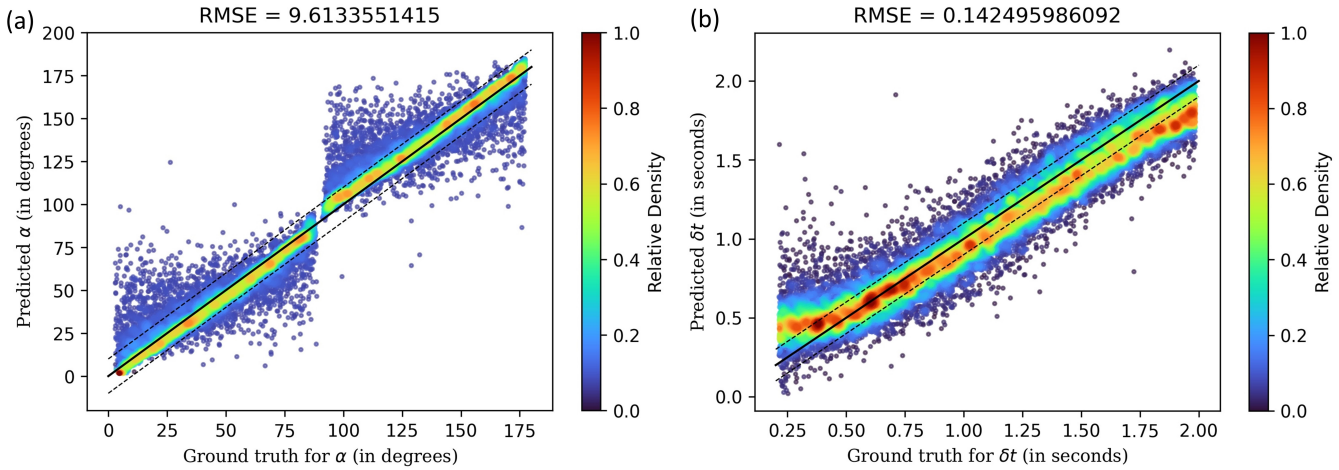

Figure S9 The performance of SWSNet on synthetic test dataset. Both the training and test datasets are contaminated by gaussian noise, with noise level chosen from a random normal distribution with mean 30% and standard deviation 10%.

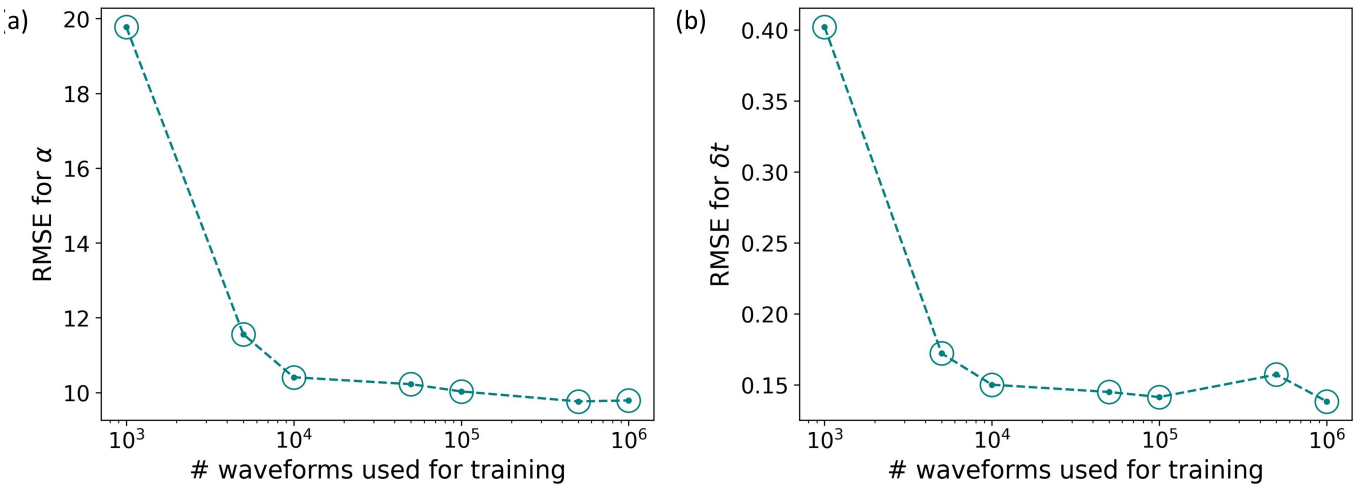

Figure S8 Variation of (a) RMSE for α (b) RMSE for δt with the size of the dataset used to train the model

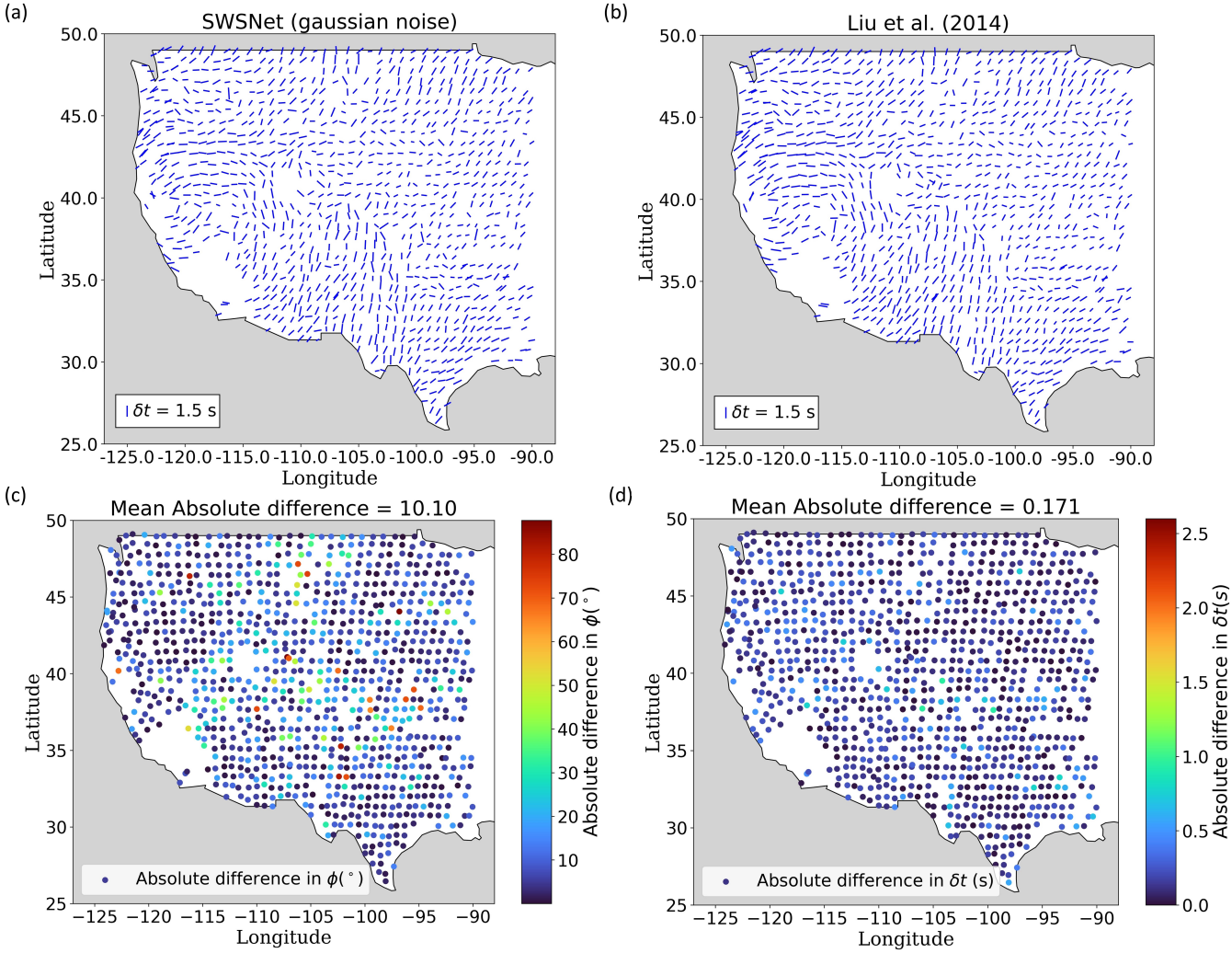

Figure S10 (a) A visual representation of the splitting parameters calculated by SWSNet trained on synthetic data with gaussian noise (b) A visual representation of the splitting parameters calculated by Liu et al. (2014). The orientation of the straight lines is representative of the fast axis orientation while the length represents delay time. Similar general pattern is observed in both cases. (c) Station-wise comparison between ϕ calculated by SWSNet (trained on data with gaussian noise) and Liu et al. (2014) (d) Station-wise comparison between δt calculated by SWSNet (trained on data with gaussian noise) and Liu et al. (2014)

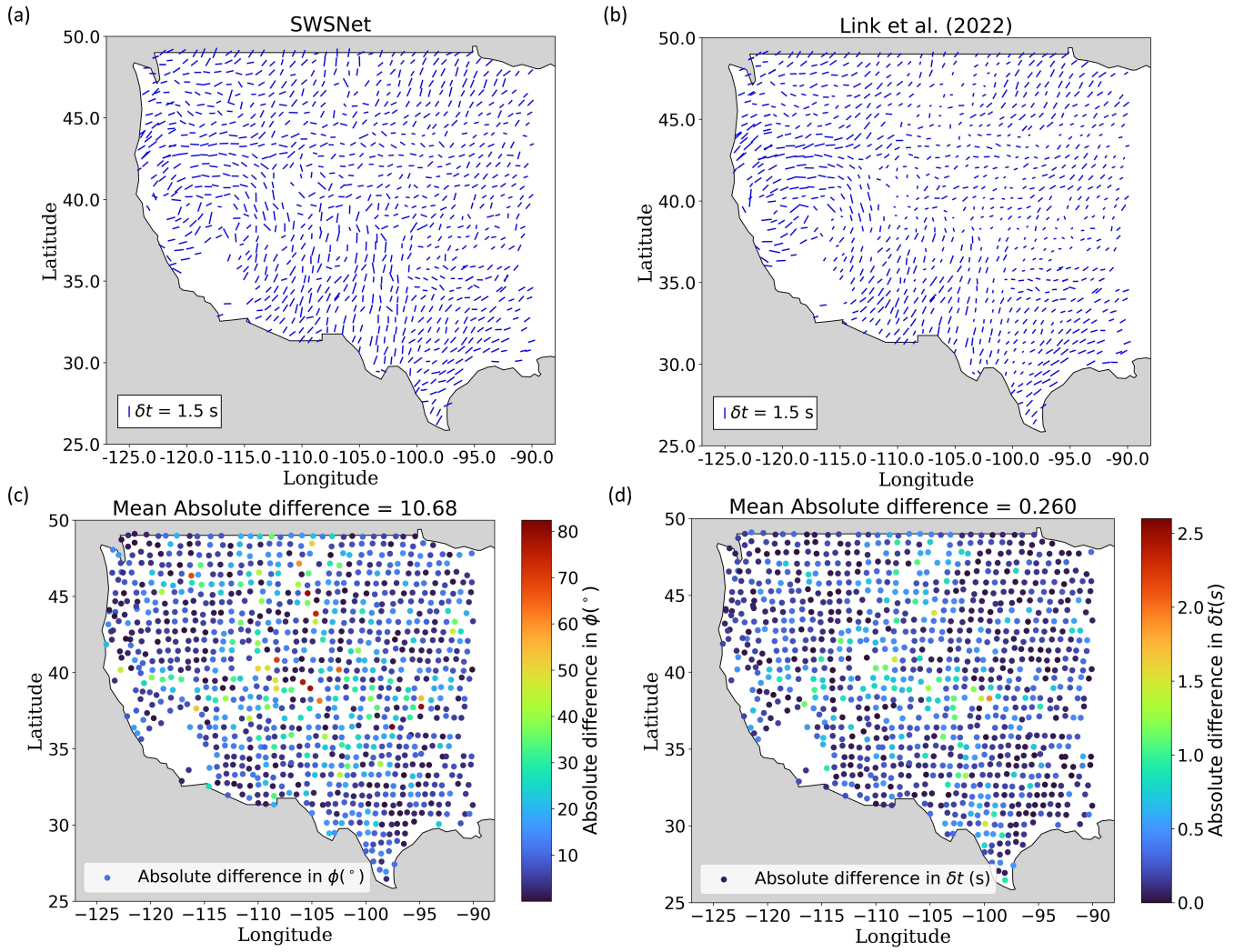

Figure S11 (a) A visual representation of the splitting parameters calculated by SWSNet (b) A visual representation of the splitting parameters calculated by Link et al. (2022) The orientation of the straight lines is representative of the fast axis orientation while the length represents delay time. Similar general pattern is observed in both cases. (c) Station-wise comparison between ϕ calculated by SWSNet and Link et al. (2022) (d) Station-wise comparison between δt calculated by SWSNet and Link et al. (2022)

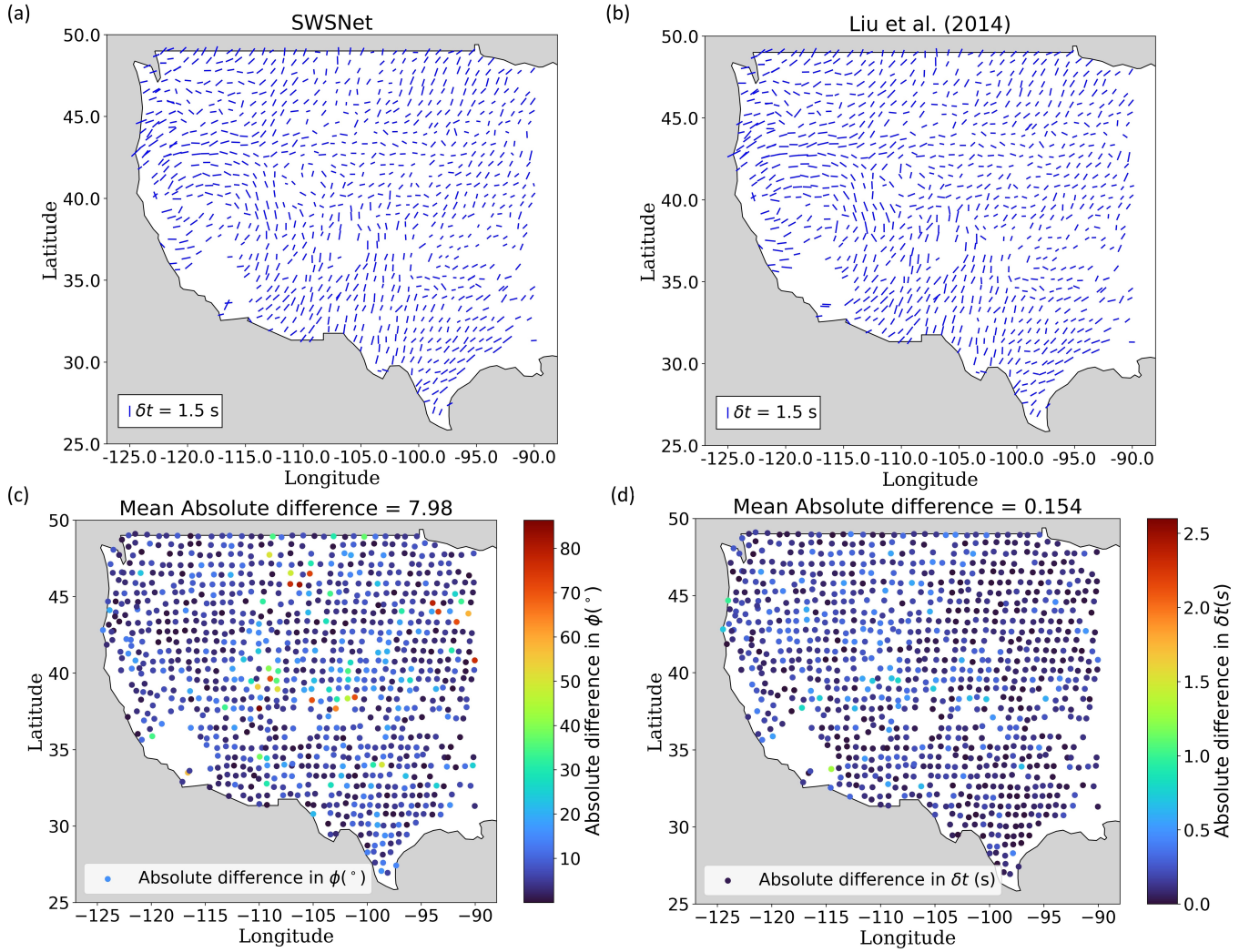

Figure S12 Splitting parameters calculated by (a) SWSNet and (b) Liu et al. (2014) for a subset of waveforms present in both datasets; Station-wise comparison between (c) ϕ and (d) δt calculated by SWSNet and Liu et al. (2014) for this subset.

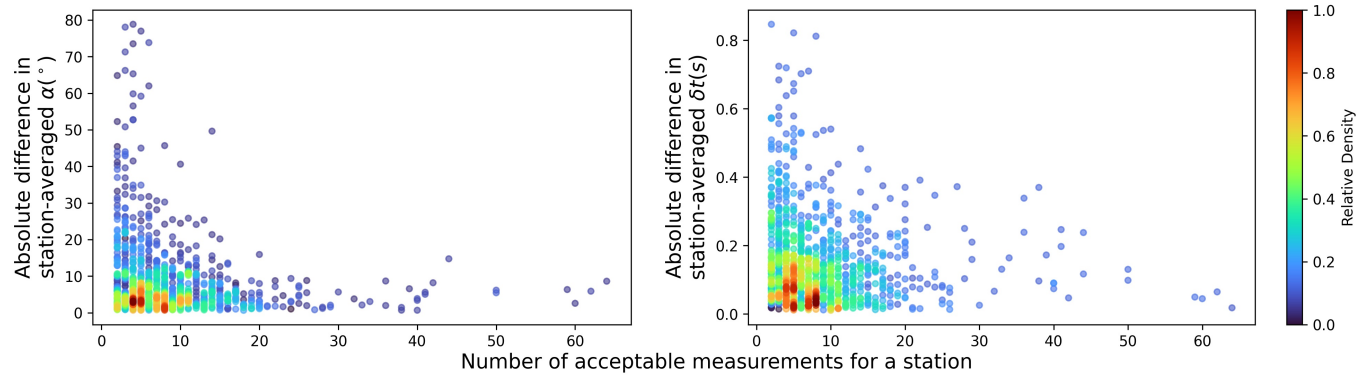

Figure S13 Variation of absolute difference between station-averaged splitting parameters calculated by SWSNet and those calculated by Liu et al. (2014), with the number of acceptable measurements for a given station. The difference decreases with increasing number of measurements

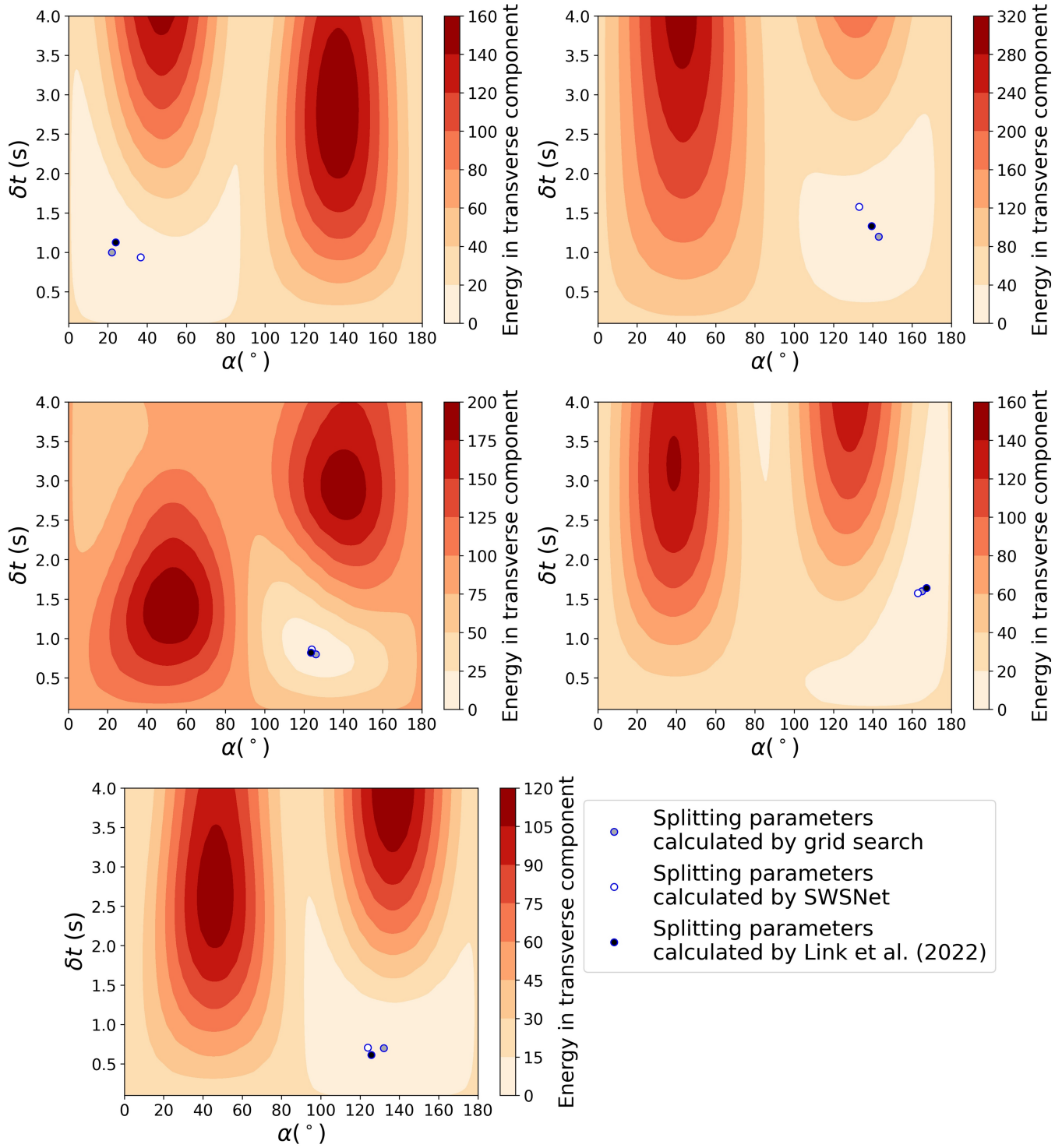

Figure S14 The distribution of transverse component energy upon inverse splitting analysis for different combinations splitting parameters for five different waveforms from five different stations.

This is a non-peer reviewed manuscript submitted to SEISMICA

Table S1 A comparison between splitting parameters for individual waveforms shown in Figure 3, calculated by grid search, Link et al. (2022) and SWSNet. Grid search 1 and 2 refer to grid searches performed on resampled raw data and deconvolved data respectively.

Event ID	$\phi(^\circ)$ (Grid Search 1)	$\phi(^\circ)$ (Grid Search 2)	$\phi(^\circ)$ (Link et al., 2022)	$\phi(^\circ)$ (SWSNet)	δt (s) (Grid Search 1)	δt (s) (Grid Search 2)	δt (s) (Link et al., 2022)	δt (s) (SWSNet)
Y13A2008-05-09T22:15:04SKS	46.5	52.5	45.0	49.1	1.33	1.11	1.20	0.90
P59A2014-08-18T02:55:43SKS	85.3	81.3	86.0	88.4	0.82	0.80	0.80	0.70
121A2018-07-13T10:10:08SKS	15.5	10.5	9.0	12.7	1.03	1.03	1.00	1.00
D25K2017-07-15T12:35:42SKKS	62.7	68.7	66.0	71.5	1.44	1.50	1.20	1.20